

UniPrompt-CL: Sustainable Continual Learning in Medical AI with Unified Prompt Pools

Gyutae Oh¹ and Jitae Shin^{1*}

Department of Electrical and Computer Engineering,
Sungkyunkwan University,
Suwon 16419, Republic of Korea
alswo740012@g.skku.edu, jtshin@skku.edu

Abstract. Modern AI models are typically trained on static datasets, limiting their ability to continuously adapt to rapidly evolving real-world environments. While Continual Learning (CL) addresses this limitation, most CL methods are designed for natural images and often underperform or fail to transfer to medical data due to domain bias, institutional constraints, and subtle inter-stage boundaries. We propose UniPrompt-CL, a medical-oriented Prompt-based Continual Learning method that improves prompt pool design via a minimally expanding unified prompt pool and a new regularization term, achieving a better stability–plasticity trade-off with lower computational cost. Across two domain-incremental learning settings, UniPrompt-CL effectively reduces inference cost while improving AvgACC by 1–3 percentage points. In addition to strong performance, extensive experiments clearly validate the motivation and effectiveness of the proposed improvements.

Keywords: Domain Incremental Learning · Prompt Based Continual Learning · Medical Artificial Intelligence

1 Introduction

Modern AI models are typically trained on static datasets, which imposes a structural limitation in continuously adapting to rapidly evolving real-world environments. To overcome this limitation, Continual Learning (CL) has been proposed. However, most CL methods have been developed and validated primarily on natural-image benchmarks, and therefore do not sufficiently reflect key characteristics of medical data (e.g., domain bias, institutional constraints, and subtle boundaries between disease stages). As a result, many existing CL approaches are difficult to apply directly to medical datasets or exhibit notable performance degradation. A central challenge is that medical images require different prompt-learning strategies than natural images. To support this claim, Fig. 1 provides

* Corresponding author: jtshin@skku.edu

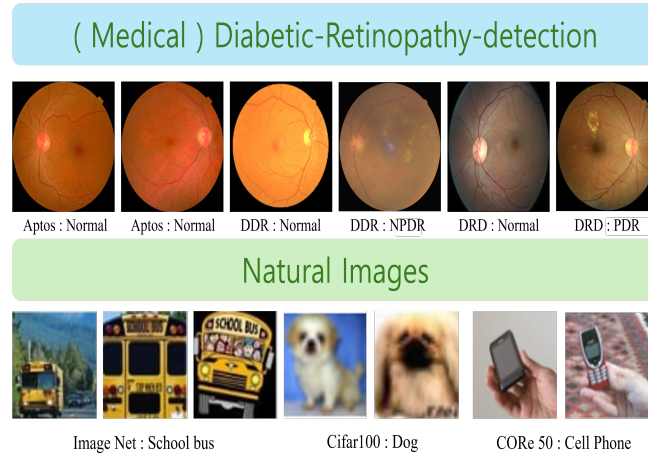


Fig. 1: To support our claim, we visualized representative examples from the natural images used in prior PCL methods and the medical datasets employed in this study.

a comparative analysis between representative natural-image datasets and medical datasets. For natural images, we reference benchmarks commonly used in prior PCL research [5, 15, 33, 37], including ImageNet [11], CIFAR100 [19], and CORE50 [22]. For medical images, we use the datasets adopted in this work, namely APTOS [12], DDR [21], and DRD [8]. As shown in Fig. 1, medical images are often collected under standardized acquisition protocols, resulting in largely consistent capture angles. Nevertheless, subtle variations arise from equipment differences, hospital-specific procedures, and patient-specific factors. Moreover, accurate diagnosis requires tracking fine-grained lesions, such as those observed in DDR (NPRD) and DRD (PRD). These observations suggest that prompt learning for medical CL should be tailored to capture subtle variations in color and lesion details. This claim is further supported by representative skin-cancer examples in Sup.fig. 4.

In contrast, natural images exhibit substantial intra-class variability in viewpoint, shape, and appearance. Accordingly, prompt-based continual learning (PCL) methods developed for natural images often learn wide prompt regions to accommodate broad feature differences, as evidenced by the widely dispersed layer-wise prompt distributions in Fig. 2.a. However, this behavior can be inefficient for medical data, where fundamental anatomical structures remain consistently important across layers and tasks. Moreover, with layer-wise independent prompt pools, similar low-level information can be repeatedly encoded at multiple layers, resulting in cross-layer redundancy and inefficient use of limited prompt capacity—as suggested by the overlapped prompt regions highlighted in Fig. 2.a. In addition, many existing PCL methods rely on multiple backbones or repeated Vision Transformer (ViT) inferences (e.g., a second forward pass

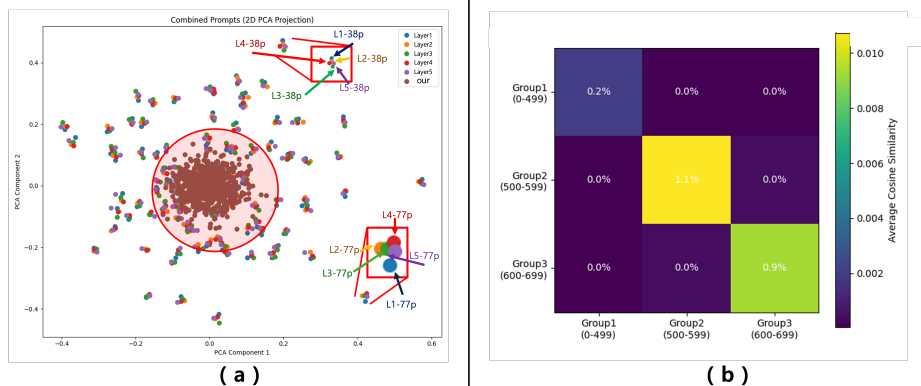


Fig. 2: (a) visualizes the prompts learned by the independent prompt pool of OS-Prompt [15] and those produced by our proposed integrated pool. The dots corresponding to layers 1-5 represent the layer-wise prompts of OS-Prompt, whereas the brown dots (Ours) denote the prompts generated by our integrated pool (see the top-right legend for details). (b) further shows that, as training progresses, newly added prompts avoid redundant or overlapping representations, indicating that each prompt captures distinct and complementary features.

or extra query-generation steps), which introduces considerable computational overhead [23, 33, 37].

Motivated by these observations, we propose UniPrompt-CL, a medical-oriented PCL method that focuses on improving prompt pool design for efficient and robust continual learning. Based on preliminary results showing consistent underperformance of prior PCL approaches on medical datasets, we posit that prompt pool design is a key bottleneck in medical PCL. UniPrompt-CL introduces (i) a unified prompt pool with minimal expansion and (ii) a novel regularization term to promote stable yet adaptive learning, achieving a better stability-plasticity trade-off than prior methods. Importantly, UniPrompt-CL attains these gains with a single backbone and a single forward pass, avoiding the need for two ViT backbones or repeated inference, thereby delivering higher accuracy at lower computational cost.

Contributions. The main contributions of this work are as follows:

- We consolidate layer-wise prompt pools into a unified prompt pool and propose a new regularization term to train it effectively.
- Our single-backbone, single-inference design substantially reduces computational cost, yet achieves superior performance over prior state-of-the-art (SOTA) methods that rely on multiple backbones or repeated ViT inferences.
- We introduce a medical-domain PCL strategy that expands only a small subset of prompts to mitigate redundancy and alleviate catastrophic forgetting.

2 Related Work

To position our work within the landscape of CL, we review recent surveys [26,35] and categorize existing methods into four main classes. **Regularization Based Methods:** Regularization based approaches introduce penalty terms into the loss function to encourage the model to retain important weights from previous tasks. Examples include Elastic Weight Consolidation (EWC) [17] and Synaptic Intelligence [41], which estimate the importance of each parameter and penalize changes proportionally [25,34]. While effective on low dimensional or simple datasets, these methods struggle when data complexity and dimensionality increase, as the approximation of parameter importance becomes unreliable. **Architecture Based Methods:** Architecture based strategies dynamically adapt the network structure to accommodate new tasks. Techniques such as Progressive Neural Networks and Supermasks allocate new subnetworks or masks per task, offering strong scalability [9,38]. However, they incur growing memory and computation costs with each new task, making them less practical for long sequences of tasks or resource-constrained environments. **Rehearsal Based Methods:** Rehearsal based approaches store a small buffer of past examples and replay them alongside new data to prevent forgetting. Methods like iCaRL [27] and Dark Experience Replay [3] have demonstrated strong performance on image benchmarks [31,39]. Yet, the need to store real data raises serious privacy and storage concerns particularly acute in the medical domain, where data sharing is heavily restricted. **PCL Methods:** PCL method fixes the majority of the pretrained model’s parameters and learns only a small set of prompt vectors for each task. This design preserves existing knowledge while adapting efficiently to new domains, drastically reducing both memory and computation overhead [5,15,33,37]. These methods have shown promise on natural-image benchmarks but often require multiple ViT inferences and have not yet been widely explored for medical data.

The Need for Medical Domain PCL: In summary, while regularization, architecture, and rehearsal methods each bring valuable insights, their applicability in the medical domain is limited by data complexity, resource constraints, and privacy issues. Prompt-based methods offer an appealing alternative by leveraging a fixed backbone and learning lightweight prompts.

3 Preliminary

The primary goal of this paper is to address the aforementioned limitations of prior PCL methods by proposing a prompt-pool learning strategy tailored to the medical domain. With this design, we aim to achieve comparable or higher performance in Domain-Incremental Learning (DIL) without relying on multiple backbones or repeated inference. As noted earlier, we adopt a PCL approach to solve these issues. Our proposed methodology builds upon the recently introduced One-Stage PCL framework [15], extending it with key improvements. While all unspecified settings follow those in the referenced work, **our approach**

differs in two main aspects: (1) it achieves high performance with only a single ViT inference, and (2) it introduces a unified prompt-pool design and training strategy tailored to medical data, inspired by insights from our experiments.

Prompt-based Continual Learning (PCL) : To understand this paper, it is important to examine the foundational OS-Prompt framework and its extended version, OS-Prompt++ [15]. Both frameworks aim to overcome the limitations of existing PCL methods. Traditional PCL approaches often incur high computational costs due to the use of an additional query function (e.g., a ViT) to generate prompt queries. To address this, OS-Prompt was proposed as a lightweight alternative that eliminates the query function, thereby significantly reducing computational overhead. The process operates as follows:

$$q_l = x_{l[\text{CLS}]}, \quad q_l \in \mathbb{R}^{1 \times D} \quad (1)$$

Where, $x_l \in \mathbb{R}^{N \times D}$ denotes the input token embeddings at layer l , N is the number of input tokens and D is the embedding dimension. To select prompts from the existing prompt pool, a cosine similarity based weighted sum is used. The prompt key matrix K_l is formed by stacking the L_p prompt key vectors $[k_l^1, k_l^2, \dots, k_l^{L_p}]$ and transposing, yielding a matrix in $\mathbb{R}^{L_p \times D}$. Where, L_p is the total number of prompts, k_l^m is the key vector of the m -th prompt ($k_l^m \in \mathbb{R}^{1 \times D}$), and the corresponding prompt value vector is $p_l^m \in \mathbb{R}^{1 \times D}$. Using the cosine similarity function $\gamma(\cdot)$, the selected prompt is computed as follows.

$$\hat{\phi}_l = \sum_{m=1}^{L_p} \gamma(q_l, k_l^m) p_l^m, \quad \hat{\phi}_l \in \mathbb{R}^{1 \times D} \quad (2)$$

However, OS-Prompt relies solely on a single [CLS] token from an intermediate layer, which limits its representational capacity and leads to only modest performance gains. To address these limitations, OS-Prompt++ requires an additional step during training: reintroducing query functionality to enhance the expressiveness of the [CLS] token. In other words, OS-Prompt++ still requires two ViT inferences during the learning process, making it difficult to consider it a true single-backbone solution.

4 Proposed Method

Our primary objective is to achieve superior CL performance with a single backbone. To this end, our methodology is built upon three key components: (1) a unified prompt pool, (2) a minimal prompt expansion strategy, and (3) a consistency-enforcing regularization term. As shown in Table 8 and Table 9 of Sup. B, medical datasets often exhibit severe long-tailed class distributions, which exacerbate catastrophic forgetting as training stages progress. To address this issue, we adopted the powerful DINOv2 backbone [24] and selected **DINOv2-base (86.6M parameters)** for its balanced trade-off between representational capacity and computational efficiency. For further details, please

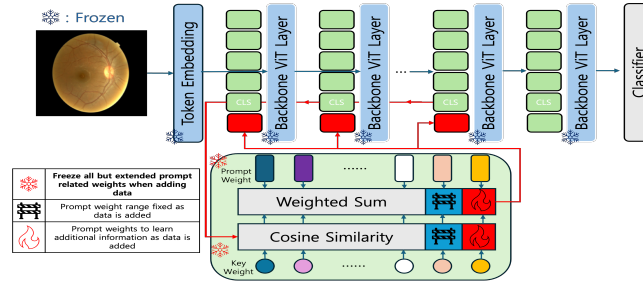


Fig. 3: This figure presents the overall architecture proposed in this study, which integrates an enhanced prompt pool. At each layer, the [CLS] token serves as a query, and the resulting layer-wise queries are centrally managed through the prompt pool integration module. This integration generates the prompts for the subsequent layer, which are then combined with x_l and propagated forward. Additionally, at each training stage, only a small number of new prompts are introduced through a minimal prompt expansion mechanism, while all previously learned prompts remain frozen.

refer to Table 12 in Sup. D. Our experiments demonstrate that this strong backbone, combined with our prompt-based design and regularization, effectively mitigates both data imbalance and catastrophic forgetting in medical CL scenarios. The overall architecture of our approach is illustrated in Fig. 3, and a concise algorithmic summary is provided in Sup. E. Algorithm 1

4.1 Motivation for Proposal and Integration of Prompt-Pool

Motivation: Prior studies [6, 10, 20] report that medical images are acquired under standardized protocols and that accurate diagnosis often depends on tracking subtle lesions. Motivated by these findings, we hypothesize that prompt learning for medical imaging should enable fine-grained adjustments. However, as analyzed in Fig. 2.a, existing PCL methods tend to learn widely dispersed prompts, and layer-wise independent prompt pools can lead to inefficient use of limited prompt capacity due to cross-layer redundancy. To address this, we propose a unified prompt pool shared across all layers, which promotes efficient prompt utilization and maximizes fine-grained feature tracking throughout the hierarchical backbone.

Method: Having established the motivation, we now describe the structure of our Integration of Prompt-Pool. Following Equation (1), we use the [CLS] token embedding of each layer as the prompt query q_l . The prompt keys are unified and defined as $k^m \in \mathbb{R}^{1 \times D}$, and the prompt value vectors are unified and defined as $p^m \in \mathbb{R}^{1 \times D}$. Consequently, the prompt computation is reformulated as follows:

$$\phi_l = \sum_{m=1}^{L_p} \gamma(q_l, k^m) p^m, \quad \phi_l \in \mathbb{R}^{1 \times D}. \quad (3)$$

The resulting prompt ϕ_l is then unified with the layer transformation:

$$x_{l+1} = f_l(x_l, \phi_l). \quad (4)$$

4.2 Few Prompt Expansion

In this subsection, we introduce the Few Prompt Expansion strategy. This strategy serves as an alternative to multi-ViT inference, maximizing the use of existing prompt information while enabling the acquisition of additional knowledge required for domain expansion. When transitioning to the next CL stage (dataset), we first construct and train the integrated prompt pool as described in Section 4.1, and then freeze the prompt weights corresponding to the previous stages. Next, the prompt set is expanded by adding 20% of the original L_p prompts. This ratio was empirically determined in Table 7. The newly added prompts are denoted as ψ , resulting in a total of $L_p + \psi$ prompts at each stage. The combined set of prompts is represented as \hat{L}_p , whose size varies depending on the stage. However, the newly added prompts (ψ) may initially have less influence compared to well-trained prompts, which can limit their learning effectiveness. To address this issue, we introduce the following formulation to ensure that the added prompts more effectively capture new information.

$$z_l = \text{Softmax}\left(\frac{K p_l^\top}{\|K\|_2 \|p_l\|_2}\right), \quad z_l \in \mathbb{R}^{B \times \hat{L}_p}, \quad (5)$$

We then refine this to:

$$S_{b,m} = 1 - z_{b,m}, \quad \mathcal{L}_s = \frac{1}{B \times \hat{L}_p} \sum_{b=1}^B \sum_{m=1}^{\hat{L}_p} S_{b,m}, \quad (6)$$

where B is the batch size and \hat{L}_p the total number of prompts.

Finally, the overall loss function is defined as:

$$\mathcal{L}_{\text{total}} = \mathcal{L}_{\text{CE}} + \lambda \mathcal{L}_s, \quad (7)$$

where λ is a hyperparameter set to 0.001 in this study to control the strength of the regularization term. The value of λ is further discussed in detail in the ablation study.

5 Experiment Settings

In this section, we describe our experimental setup in detail to substantiate our claims. First, we introduce the datasets used in our experiments; second, we outline the data augmentation and preprocessing methods, baseline validation procedures, evaluation metrics, and implementation environment. Detailed information about the datasets and the experimental settings can be found in Sup. B.

Continual Learning Problem Setting & Dataset: We simulate a hospital-driven Domain-Incremental Learning (DIL) setting with unknown task identities, following a rehearsal-free protocol where data from past/future stages are inaccessible [35]. Our main experiments use diabetic retinopathy datasets with unified three-class labels [18] (APTOS [12] \rightarrow DDR [21] \rightarrow DRD [8]). For generalization, we additionally evaluate on skin cancer datasets (ISIC [29] \rightarrow HAM [7] \rightarrow DERM7 [13]); example images and further details are provided in Sup. B.

Experimental Details: During training, we apply random data augmentations, including HorizontalFlip, Rotation, and VerticalFlip. For ViT preprocessing, we use AutoImageProcessor from the transformers library with facebook/dinov2-base weights. We validate baseline methods using rigorously implemented CL libraries [2, 3], and implement any additional required components ourselves.

For a more rigorous evaluation, we report not only standard continual learning metrics (AvgACC \uparrow , BWT \uparrow , and AvgF \downarrow), but also (i) an overall performance-change table and (ii) Cost-Adjusted Retained Accuracy (CARA) to quantify the trade-off between accuracy and efficiency. CARA combines performance (AvgACC) and stability (retention = $1 - \text{AvgF}$) into a single retained performance and normalizes it by GFLOPs, summarizing the trade-off among accuracy, forgetting, and efficiency. In addition, since medical datasets often exhibit severe class imbalance, we report F1-score-based metrics to demonstrate robustness to imbalance. Detailed definitions and computation procedures for all metrics are described in Sup. C.

6 Experiment Results

In this session, to aid the readers’ understanding, we separate the results of each table and figure into individual sections and discuss them in detail.

Stage-Wise Prompt Independence and Fine-Grained Feature Encoding : As discussed in Section 4.2. Motivation, we hypothesize that prompts introduced at each stage should (i) preserve previously acquired knowledge while (ii) encoding new, fine-grained features. Fig. 2.(b) supports this hypothesis by visualizing the inter-stage prompt similarity matrix under our method. The pronounced diagonal structure indicates that prompts learned at different stages remain largely independent, exhibiting minimal redundancy across stages. In other words, newly added prompts capture novel information rather than overlapping with existing prompts. Moreover, Fig. 2.(a) suggests that our expansion strategy focuses on subtle distinctions. In the figure, the brown markers denote prompts learned by our integrated prompt pool, whereas the other colors correspond to prompts from the existing PCL method. While OS-Prompt prompts broadly cover the feature space, our integrated prompts form tighter clusters, implying more refined and discriminative representations. Finally, the quantitative results in Table 1 show consistent improvements over prior SOTA methods, providing empirical evidence for the hypothesis in Section 4.1.

Comparative Performance Analysis with State-of-the-Art (SOTA) CL Methods: Table 1 compares our method not only against strong PCL base-

Table 1: Final Accuracy (Acc) and F1-Score (F1) Results After the Final Stage and Performance Comparison with Other PCL Models. The symbol † denotes our proposed model. PCL denotes prompt-based continual learning; Arch-CL refers to architecture-based continual learning; Reh-CL means rehearsal-based continual learning; and Reg-CL indicates regularization-based continual learning. (**bold** indicates the highest performance;)

CL-Type (Ref)	Model	APTOS		DDR		DRD	
		Acc	F1	Acc	F1	Acc	F1
PCL (ECCV2024)	OS [15]	0.687±0.011	0.637±0.042	0.693±0.013	0.648±0.043	0.619±0.002	0.568±0.063
PCL (ECCV2024)	OS++ [15]	0.743±0.104	0.686±0.072	0.697±0.032	0.655±0.032	0.623±0.005	0.565±0.023
Arch-CL (CVPR2024)	MoE-Adapters [40]	0.835±0.001	0.742±0.001	0.747±0.004	0.694±0.013	0.564±0.002	0.478±0.006
PCL (CVPR2023)	Coda-Prompt [33]	0.682±0.022	0.646±0.022	0.721±0.001	0.697±0.023	0.663±0.015	0.557±0.061
PCL (ECCV2022)	Dual-prompt [36]	0.363±0.044	0.185±0.002	0.435±0.003	0.222±0.012	0.604±0.042	0.259±0.001
Reh-CL (NIPS2020)	DER++ [3]	0.531±0.213	0.442±0.253	0.609±0.152	0.567±0.284	0.681±0.043	0.612±0.072
Reg-CL (ICML2018)	Online EWC [30]	0.746±0.003	0.695±0.003	0.702±0.002	0.708±0.002	0.698±0.006	0.653±0.004
-	UniPrompt-CL†	0.849±0.011	0.761±0.002	0.772±0.032	0.723±0.042	0.701±0.005	0.656±0.001

lines but also against representative non-PCL families (architecture-modified, rehearsal-based, and regularization-based), reporting the final-stage accuracy and F1-score on each dataset. Overall, our method consistently achieves the highest accuracy and F1-score, demonstrating superior continual learning performance in the medical imaging domain. These gains can be interpreted through the characteristics of medical images (Fig. 1) and the corresponding prompt-learning behavior as well as the resulting prompt distribution (Fig. 2.a). Prior SOTA PCL methods, largely designed for natural images, tend to learn wide prompt regions. As shown in Fig. 2.a, their layer-wise prompts often overlap and form similar distributions across layers. This tendency suggests that the model may repeatedly encode identical or highly similar low-level features at multiple layers, which can lead to inefficient use of limited prompt capacity due to redundant re-encoding. In contrast, medical images are acquired under standardized protocols, yielding relatively consistent anatomical structures, and the key factors for performance are subtle variations such as device/institution/patient-dependent color shifts and fine-grained lesions (Fig. 1). Therefore, in medical settings, a compact and fine-grained prompt distribution that allocates limited prompt capacity to medically relevant details can be more appropriate than broadly spread prompt clusters. Our method addresses this issue via a global integrated prompt pool that reduces cross-layer redundancy and expands prompts only minimally when necessary. The more compact prompt distribution observed in Fig. 2.a is consistent with this design choice and aligns with the improvements in accuracy and F1-Score reported in Table 1. Taken together, these findings underscore the need for domain-specific learning strategies: prompt representations that work well for natural images do not necessarily transfer to medical data, and adapting prompt distributions and learning schemes to the characteristics of medical data can lead to improved continual learning performance.

Stage-Wise Forgetting Mitigation and Performance Gains: In this section, we describe the performance comparison results presented in Table 2. Table 2 builds upon the results of Table 1 and illustrates how accuracy and F1-score change across learning stages, with OS-Prompt++, the best-performing

Table 2: Tracking and comparing various catastrophic forgetting outcomes during stage progression (where **Red** indicates data learned at the current step, **Blue** indicates previously learned data (seen), and Black indicates unseen data) [Accuracy (Acc), F1-score (F1), OS prompt++ (OS++); **Horizontal: Training Data, Vertical: Evaluation Data**]. Additionally, the FLOPs row indicates the amount of computing resources used. The symbol † denotes our proposed model.

		Evaluation											
		OS-Prompt++ (Dual inference)						UniPrompt-CL† (Single inference)					
Training Dataset		APTOS		DDR		DRD		APTOS		DDR		DRD	
		Acc	F1	Acc	F1	Acc	F1	Acc	F1	Acc	F1	Acc	F1
Stage 1	APTOS	0.868	0.753	0.565	0.474	0.409	0.354	0.901	0.767	0.601	0.447	0.453	0.381
Stage 2	DDR	0.707	0.638	0.797	0.748	0.508	0.413	0.866	0.663	0.878	0.844	0.636	0.534
Stage 3	DRD	0.743	0.686	0.697	0.655	0.623	0.565	0.849	0.761	0.772	0.723	0.701	0.656
FLOPs		66.42 GFLOPs						44.17 GFLOPs					

prompt-based continual learning method in Table 1, serving as the baseline. The most notable observation in Table 2 is that the proposed method not only mitigates catastrophic forgetting effectively but also improves overall performance. Moreover, while OS-Prompt++ relies on two ViT inferences, our approach achieves superior performance with only a single ViT inference. Furthermore, even when employing expanded prompts, our method requires only one ViT inference, thereby significantly reducing GFLOPs and demonstrating high computational efficiency.

Table 3: Performance evaluation of AvgACC, BWT, and Cost-Adjusted Retained Accuracy (CARA) across three diabetic retinopathy datasets. Training-time GFLOPs (per step, including forward and backward passes). The symbol † denotes our proposed model. The best results are highlighted in **bold**.

Method	AvgACC↑	BWT↑	AvgF↓	GFLOPs↓	CARA _{0.5} ↑
OS-Prompt	0.666±0.062	-0.132±0.003	0.132±0.003	34.26	0.098
MoE-Adapters	0.716±0.141	-0.080±0.092	0.080±0.092	105.64	0.064
Coda-Prompt	0.688±0.079	-0.140±0.044	0.140±0.044	134.33	0.051
Dual-prompt	0.467±0.159	-0.291±0.065	0.291±0.065	105.05	0.032
DER++	0.607±0.121	-0.288±0.160	0.288±0.160	168.02	0.033
Online EWC	0.715±0.151	-0.174±0.002	0.174±0.002	100.62	0.059
OS-Prompt++ (Original)	0.769±0.027	-0.113±0.006	0.113±0.006	51.12	0.095
OS-Prompt++ (Add Dino-v2)	0.812±0.023	-0.125±0.052	0.125±0.052	66.42	0.087
UniPrompt-CL†	0.844±0.016	-0.079±0.032	0.079±0.032	44.17	0.116

Quantitative validation using forgetting metrics: In this subsection, we evaluate all models appearing in Tables 1 using both standard CL metrics and the CARA. A higher CARA indicates more stable and efficient per-

Table 4: Performance evaluation of AvgACC and BWT across three small external skin cancer datasets. The symbol † denotes our proposed model.

Model	AvgACC \uparrow	BWT \uparrow	AvgF \downarrow	GFLOPs \downarrow	CARA $_{0.5}$ \uparrow
OS	0.682 \pm 0.041	-0.135 \pm 0.075	0.135 \pm 0.075	34.26	0.101
OS++	0.725 \pm 0.032	-0.063 \pm 0.013	0.063 \pm 0.013	51.12	0.095
MoE-Adapters	0.597 \pm 0.165	-0.040 \pm 0.016	0.040 \pm 0.016	105.64	0.056
Coda-Prompt	0.713 \pm 0.040	-0.041 \pm 0.013	0.041 \pm 0.013	134.33	0.059
Dual-prompt	0.637 \pm 0.065	-0.012\pm0.039	0.012\pm0.039	105.05	0.061
DER++	0.722 \pm 0.057	-0.099 \pm 0.023	0.099 \pm 0.023	168.02	0.050
Online EWC	0.708 \pm 0.054	-0.157 \pm 0.002	0.157 \pm 0.002	100.62	0.060
UniPrompt-CL †	0.732\pm0.022	-0.049 \pm 0.043	0.049 \pm 0.043	44.17	0.105

formance in standard CL per unit GFLOPs. The definitions and computation procedures for the standard metrics and CARA are summarized in Appendix C. As shown in Table 3, our method generally outperforms PCL, regularization, rehearsal, and architecture-based baselines. Notably, it consistently surpasses the backbone-strengthened PCL, suggesting that the gains stem from the fixed-ratio few-prompt expansion and the unified prompt-pool design. Finally, from the CARA perspective, our approach exceeds all SOTA methods, demonstrating the best performance to GFLOPs efficiency. The best results in Table 3 are highlighted in **bold**.

External Validation on Additional Datasets: To further verify that our framework is not restricted to diabetic retinopathy (DR) but is generally applicable to medical imaging tasks, we additionally conduct a small-scale pilot study on skin cancer classification. Specifically, we construct a continual learning scenario using three dermatology datasets, and detailed settings are provided in Sup. B. In this setting, our method achieves the highest AvgACC on the skin cancer benchmarks, indicating that the proposed framework can transfer beyond DR and remains effective on a distinct disease and imaging domain. While our BWT/AvgF are sometimes slightly below a few baselines—indicating mild forgetting the overall utility is decisively better once compute is accounted for: Our method attains the highest AvgACC (0.732) at single-pass 44.17 GFLOPs, and its cost-adjusted retained accuracy CARA $_{0.5}$ = 0.105 surpasses strong PCL baselines—OS (0.101), OS++ (0.095), and Coda-Prompt (0.059)—and also exceeds representative non-PCL families, including rehearsal-based DER++ (0.05), regularization based Online EWC (0.06), and architecture-based MoE-Adapters (0.056). A complete summary of all models (AvgACC, BWT, AvgF, GFLOPs, and CARA $_{0.5}$) is provided in Table 4. In short, on a per-compute basis our method retains and delivers more accuracy, making the modest gaps in forgetting metrics a reasonable, principled trade-off rather than a substantive limitation.

7 Ablation Study

In this section, we conduct ablation studies to improve interpretability and reliability by clarifying the causal factors behind performance gains. Our objective is to pinpoint directions for model improvement and explicitly highlight the key contributing components.

Table 5: We compare the results of fatal forgetting during the stepwise progression of the baseline model, the introduction of a stronger backbone, and the methodology of this study. Through these exclusion studies, we highlight the importance of a good backbone in PCL and show that there is room for further improvement. It can be interpreted in the same way as Table 2.

OS-Prompt++ (Original)						
	APTOS		DDR		DRD	
	Acc	F1	Acc	F1	Acc	F1
APTOS	0.868	0.753	0.565	0.474	0.409	0.354
DDR	0.707	0.638	0.797	0.748	0.508	0.413
DRD	0.743	0.686	0.697	0.655	0.623	0.565
OS-Prompt++ (Add Dino-v2)						
	APTOS		DDR		DRD	
	Acc	F1	Acc	F1	Acc	F1
APTOS	0.918	0.823	0.608	0.520	0.492	0.467
DDR	0.732	0.604	0.849	0.828	0.625	0.563
DRD	0.754	0.690	0.763	0.721	0.668	0.585
UniPrompt-CL[†](Proposed)						
	APTOS		DDR		DRD	
	Acc	F1	Acc	F1	Acc	F1
APTOS	0.901	0.767	0.601	0.447	0.453	0.381
DDR	0.866	0.663	0.878	0.844	0.636	0.534
DRD	0.849	0.761	0.772	0.723	0.701	0.656

Effectiveness of Strong Backbones in Prompt-Based Continual Learning: In Table 5, we demonstrate both the necessity of incorporating a powerful backbone into PCL and that our method’s superior performance cannot be attributed to the backbone alone. We examine foundation models such as Dino-V2 because, unlike conventional backbones, these models are pretrained on massive datasets and are capable of extracting high-quality features across diverse tasks. Although several prior studies have utilized foundation models to achieve outstanding few-shot and zero-shot performance [1, 14, 16, 28, 32], their applicability

within the PCL domain remains underexplored. Given the severe class imbalance and limited sample sizes commonly observed in the medical domain, we anticipated greater performance gains from adopting a foundation model. Accordingly, to test our hypothesis fairly within the PCL paradigm, we use OS-Prompt++ the top-performing PCL method in Table 1 as our baseline for comparison.

- Original OS-Prompt++ (without backbone enhancement)
- OS-Prompt++ with a Dino-V2 backbone
- Our proposed method

To ensure a fair comparison, all experimental conditions were held constant except for the backbone. Comparing the original OS-Prompt++ with its Dino-V2 variant, we observe that the incorporation of Dino-V2 improves both overall accuracy and robustness against forgetting. This result indicates that a stronger backbone provides generalization benefits analogous to few-shot and zero-shot learning, even within PCL settings. Importantly, our full method still outperforms both variants, demonstrating that the gains achieved by Few Prompt Expansion and Integration of the Prompt Pool extend beyond what can be attributed to backbone strength alone.

Table 6: We compare the performance with and without \mathcal{L}_s under various values of λ (Eq. 7). The FAA and FAF after the last stage are reported.

\mathcal{L}_s	λ	FAA	FAF
\times	\times	0.754	0.701
\checkmark	0.01	0.777	0.705
\checkmark	<u>0.001</u>	<u>0.775</u>	0.713
\checkmark	0.0001	0.765	0.723

Impact of the Proposed Loss Term: In this subsection, we evaluate the performance impact of the loss term proposed in Section 4.2. The results are presented in Table 6, where all metrics are measured after the final training step. Where, FAA denotes the Final Average Accuracy across all stages, and FAF indicates the Final Average F1-score across all stages. The hyperparameter configurations follow the settings listed in Sup. Table 10. First, the results obtained without the proposed loss term consistently show performance degradation compared to those with the loss term applied. This confirms that the proposed loss operates as intended, demonstrating robustness and efficiency, while also suggesting potential for further improvement. Furthermore, we analyze the effect of the λ value used in the loss formulation. Interestingly, larger values of λ tend to increase FFA, whereas smaller values of λ tend to increase FAF. Since both metrics are equally important, we finally adopt $\lambda = 0.001$ as a balanced choice.

Impact of Prompt Expansion Ratio on Continual Learning Performance: In this subsection, we discuss the procedure for selecting the prompt expansion ratio. We evaluated candidate ratios of 10%, 20%, and 30%, and the

Table 7: Performance Evaluation by Prompt Expansion Ratio. ♣ denotes the expansion ratio we selected.

# Prompt Extensions	Stage (Training Dataset)	APTOS		DDR		DRD	
		Acc	F1	Acc	F1	Acc	F1
50 (10%)	Stage 1 (APTOS)	0.898	0.765	0.592	0.440	0.446	0.372
	Stage 2 (DDR)	0.830	0.659	0.868	0.852	0.630	0.534
	Stage 3 (DRD)	0.803	0.751	0.739	0.706	0.692	0.659
100 (20%) ♣	Stage 1 (APTOS)	0.901	0.767	0.601	0.447	0.453	0.381
	Stage 2 (DDR)	0.866	0.663	0.878	0.844	0.636	0.534
	Stage 3 (DRD)	0.849	0.761	0.772	0.723	0.701	0.656
150 (30%)	Stage 1 (APTOS)	0.901	0.774	0.608	0.469	0.470	0.408
	Stage 2 (DDR)	0.816	0.668	0.869	0.856	0.637	0.543
	Stage 3 (DRD)	0.836	0.757	0.757	0.709	0.694	0.636

results are presented in Table 7. All experiments adhered to the detailed hyperparameter settings outlined in Sup. Table 10. We ultimately selected a 20% expansion ratio because increasing from 10% to 20% yielded clear performance improvements, whereas further expanding to 30% increased the parameter count without corresponding gains and even caused slight performance degradation. These findings indicate that indiscriminate expansion of parameters does not guarantee better performance.

8 Conclusion and Future Work

Conclusion. Medical continual learning demands both strong performance under domain shifts and practical efficiency at inference time. To address this, we propose UniPrompt-CL, which combines a strong foundation backbone with efficient prompt management to mitigate catastrophic forgetting in medical AI. Motivated by the persistent underperformance of prior PCL methods on medical datasets and our analysis of prompt behavior under domain shifts, we revisit prompt pool design and introduce a medical-oriented improvement: an integrated prompt pool with lightweight expansion. We validate this design choice through comprehensive experiments and analyses. Across diabetic retinopathy and skin-cancer datasets, UniPrompt-CL improves AvgACC by 1–3 percentage points over strong baselines; in the best case, it achieves up to +10 pp in accuracy and a +9-point gain in F1 score. Moreover, it maintains a favorable efficiency-performance trade-off by reducing inference cost even when GPLOPs are taken into account, and it attains these gains with a single ViT inference—avoiding the multiple passes or complex pipelines required by prior PCL approaches. Finally, our findings underscore domain-specific considerations: because medical data are acquired under standardized protocols, prompt learning behaves differently than in natural images. While existing methods often generalize poorly to such

conditions, our integrated prompt design better preserves prior knowledge while capturing fine-grained features, leading to robust and stable performance.

Future Work. While our large-scale evaluation focused on diabetic retinopathy classification, a small-scale pilot on skin-cancer datasets also showed strong AvgACC, suggesting promising transferability. Future work will extend UniPrompt-CL to additional modalities (e.g., CT, MRI, pathology) and structured tasks (e.g., segmentation, detection) for broader validation. We also plan to explore domain-specific vision encoders (e.g., Med-CLIP or Med-ViT) to further improve efficiency and accuracy in medical applications.

References

1. Alayrac, J.B., Donahue, J., Luc, P., Miech, A., Barr, I., Hasson, Y., Lenc, K., Mensch, A., Millican, K., Reynolds, M., et al.: Flamingo: a visual language model for few-shot learning. *Advances in neural information processing systems* **35**, 23716–23736 (2022)
2. Boschini, M., Bonicelli, L., Buzzega, P., Porrello, A., Calderara, S.: Class-incremental continual learning into the extended der-verse. *IEEE Transactions on Pattern Analysis and Machine Intelligence* (2022)
3. Buzzega, P., Boschini, M., Porrello, A., Abati, D., Calderara, S.: Dark experience for general continual learning: a strong, simple baseline. In: Larochelle, H., Ranzato, M., Hadsell, R., Balcan, M.F., Lin, H. (eds.) *Advances in Neural Information Processing Systems*. vol. 33, pp. 15920–15930. Curran Associates, Inc. (2020)
4. Cassidy, B., Kendrick, C., Brodzicki, A., Jaworek-Korjakowska, J., Yap, M.H.: Analysis of the isic image datasets: Usage, benchmarks and recommendations. *Medical image analysis* **75**, 102305 (2022)
5. Chen, H., Wu, Z., Han, X., Jia, M., Jiang, Y.G.: Promptfusion: Decoupling stability and plasticity for continual learning. In: *European Conference on Computer Vision*. pp. 196–212. Springer (2024)
6. Cleland, C.: Comparing the international clinical diabetic retinopathy (icdr) severity scale. *Community eye Health* **36**(119), 10 (2023)
7. Codella, N., Rotemberg, V., Tschandl, P., Celebi, M.E., Dusza, S., Gutman, D., Helba, B., Kalloo, A., Liopyris, K., Marchetti, M., et al.: Skin lesion analysis toward melanoma detection 2018: A challenge hosted by the international skin imaging collaboration (isic). *arXiv preprint arXiv:1902.03368* (2019)
8. Dugas, E., Jared, Jorge, Cukierski, W.: Diabetic retinopathy detection. <https://kaggle.com/competitions/diabetic-retinopathy-detection> (2015), kaggle
9. Ebrahimi, S., Meier, F., Calandra, R., Darrell, T., Rohrbach, M.: Adversarial continual learning. In: *Computer Vision—ECCV 2020: 16th European Conference, Glasgow, UK, August 23–28, 2020, Proceedings, Part XI* 16. pp. 386–402. Springer (2020)
10. Guan, H., Liu, M.: Domain adaptation for medical image analysis: a survey. *IEEE Transactions on Biomedical Engineering* **69**(3), 1173–1185 (2021)
11. Howard, A., Park, E., Kan, W.: Imagenet object localization challenge. <https://kaggle.com/competitions/imagenet-object-localization-challenge> (2018), kaggle
12. Karthik, Maggie, Dane, S.: Aptos 2019 blindness detection. <https://kaggle.com/competitions/aptos2019-blindness-detection> (2019), kaggle
13. Kawahara, J., Daneshvar, S., Argenziano, G., Hamarneh, G.: Seven-point checklist and skin lesion classification using multitask multimodal neural nets. *IEEE journal of biomedical and health informatics* **23**(2), 538–546 (2018)
14. Kim, B., Shin, C., Jeong, J., Jung, H., Lee, S.Y., Chun, S., Hwang, D.H., Yu, J.: Zim: Zero-shot image matting for anything. *arXiv preprint arXiv:2411.00626* (2024)
15. Kim, Y., Li, Y., Panda, P.: One-stage prompt-based continual learning. In: *European conference on computer vision*. pp. 163–179. Springer (2024)
16. Kirillov, A., Mintun, E., Ravi, N., Mao, H., Rolland, C., Gustafson, L., Xiao, T., Whitehead, S., Berg, A.C., Lo, W.Y., et al.: Segment anything. In: *Proceedings of the IEEE/CVF international conference on computer vision*. pp. 4015–4026 (2023)

17. Kirkpatrick, J., Pascanu, R., Rabinowitz, N., Veness, J., Desjardins, G., Rusu, A.A., Milan, K., Quan, J., Ramalho, T., Grabska-Barwinska, A., et al.: Overcoming catastrophic forgetting in neural networks. *Proceedings of the national academy of sciences* **114**(13), 3521–3526 (2017)
18. Kobat, S.G., Baygin, N., Yusufoglu, E., Baygin, M., Barua, P.D., Dogan, S., Yaman, O., Celiker, U., Yildirim, H., Tan, R.S., et al.: Automated diabetic retinopathy detection using horizontal and vertical patch division-based pre-trained densenet with digital fundus images. *Diagnostics* **12**(8), 1975 (2022)
19. Krizhevsky, A.: Learning multiple layers of features from tiny images. Tech. rep. (2009)
20. Kushol, R., Wilman, A.H., Kalra, S., Yang, Y.H.: Dsmri: domain shift analyzer for multi-center mri datasets. *Diagnostics* **13**(18), 2947 (2023)
21. Li, T., Gao, Y., Wang, K., Guo, S., Liu, H., Kang, H.: Diagnostic assessment of deep learning algorithms for diabetic retinopathy screening. *Information Sciences* **501**, 511 – 522 (2019). <https://doi.org/https://doi.org/10.1016/j.ins.2019.06.011>, <http://www.sciencedirect.com/science/article/pii/S0020025519305377>
22. Lomonaco, V., Maltoni, D.: Core50: a new dataset and benchmark for continuous object recognition. In: *Proceedings of the 1st Annual Conference on Robot Learning*. vol. 78, pp. 17–26 (2017)
23. Menabue, M., Frascaroli, E., Boschini, M., Sangineto, E., Bonicelli, L., Porrello, A., Calderara, S.: Semantic residual prompts for continual learning. In: *European Conference on Computer Vision*. pp. 1–18. Springer (2024)
24. Oquab, M., Darcet, T., Moutakanni, T., Vo, H., Szafraniec, M., Khalidov, V., Fernandez, P., Haziza, D., Massa, F., El-Nouby, A., et al.: Dinov2: Learning robust visual features without supervision. *arXiv preprint arXiv:2304.07193* (2023)
25. Pham, Q., Liu, C., Hoi, S.: Continual normalization: Rethinking batch normalization for online continual learning. *arXiv preprint arXiv:2203.16102* (2022)
26. Qazi, M.A., Hashmi, A.U.R., Sanjeev, S., Almakky, I., Saeed, N., Gonzalez, C., Yaqub, M.: Continual learning in medical imaging: A survey and practical analysis. *arXiv preprint arXiv:2405.13482* (2024)
27. Rebuffi, S.A., Kolesnikov, A., Sperl, G., Lampert, C.H.: icarl: Incremental classifier and representation learning. In: *Proceedings of the IEEE conference on Computer Vision and Pattern Recognition*. pp. 2001–2010 (2017)
28. Ren, T., Chen, Y., Jiang, Q., Zeng, Z., Xiong, Y., Liu, W., Ma, Z., Shen, J., Gao, Y., Jiang, X., et al.: Dino-x: A unified vision model for open-world object detection and understanding, 2024. URL <https://arxiv.org/abs/2411.14347> **18** (2024)
29. Rotemberg, V., Kurtansky, N., Betz-Stablein, B., Caffery, L., Chousakos, E., Codella, N., Combalia, M., Dusza, S., Guitera, P., Gutman, D., et al.: A patient-centric dataset of images and metadata for identifying melanomas using clinical context. *Scientific data* **8**(1), 34 (2021)
30. Schwarz, J., Czarnecki, W., Luketina, J., Grabska-Barwinska, A., Teh, Y.W., Pascanu, R., Hadsell, R.: Progress & compress: A scalable framework for continual learning. In: *International conference on machine learning*. pp. 4528–4537. PMLR (2018)
31. Shin, H., Lee, J.K., Kim, J., Kim, J.: Continual learning with deep generative replay. *Advances in neural information processing systems* **30** (2017)
32. Singh, R., Puhl, R.B., Dhakal, K., Sornapudi, S.: Few-shot adaptation of grounding dino for agricultural domain. *arXiv preprint arXiv:2504.07252* (2025)

33. Smith, J.S., Karlinsky, L., Gutta, V., Cascante-Bonilla, P., Kim, D., Arbelle, A., Panda, R., Feris, R., Kira, Z.: Coda-prompt: Continual decomposed attention-based prompting for rehearsal-free continual learning. In: Proceedings of the IEEE/CVF Conference on Computer Vision and Pattern Recognition. pp. 11909–11919 (2023)
34. Wang, B., Luo, X., Zhuang, X.: Toward universal medical image registration via sharpness-aware meta-continual learning. In: International Conference on Medical Image Computing and Computer-Assisted Intervention. pp. 739–748. Springer (2024)
35. Wang, L., Zhang, X., Su, H., Zhu, J.: A comprehensive survey of continual learning: theory, method and application. *IEEE Transactions on Pattern Analysis and Machine Intelligence* (2024)
36. Wang, Z., Zhang, Z., Ebrahimi, S., Sun, R., Zhang, H., Lee, C.Y., Ren, X., Su, G., Perot, V., Dy, J., et al.: Dualprompt: Complementary prompting for rehearsal-free continual learning. In: European Conference on Computer Vision. pp. 631–648. Springer (2022)
37. Wang, Z., Zhang, Z., Lee, C.Y., Zhang, H., Sun, R., Ren, X., Su, G., Perot, V., Dy, J., Pfister, T.: Learning to prompt for continual learning. In: Proceedings of the IEEE/CVF conference on computer vision and pattern recognition. pp. 139–149 (2022)
38. Wortsman, M., Ramanujan, V., Liu, R., Kembhavi, A., Rastegari, M., Yosinski, J., Farhadi, A.: Supermasks in superposition. *Advances in Neural Information Processing Systems* **33**, 15173–15184 (2020)
39. Wu, C., Herranz, L., Liu, X., Van De Weijer, J., Raducanu, B., et al.: Memory replay gans: Learning to generate new categories without forgetting. *Advances in neural information processing systems* **31** (2018)
40. Yu, J., Zhuge, Y., Zhang, L., Hu, P., Wang, D., Lu, H., He, Y.: Boosting continual learning of vision-language models via mixture-of-experts adapters. In: Proceedings of the IEEE/CVF Conference on Computer Vision and Pattern Recognition. pp. 23219–23230 (2024)
41. Zenke, F., Poole, B., Ganguli, S.: Continual learning through synaptic intelligence. In: International conference on machine learning. pp. 3987–3995. PMLR (2017)

Supplementary material

Supplementary material Overview

This supplementary material provides additional details on GenAI Usage Disclosure, Implementation and Reproducibility Details, Continual Learning Metrics and CARA and Model Size Analysis: Facebook/DINOv2.

- **A. GenAI Usage Disclosure.**
Statement on the use of generative AI tools in manuscript preparation.
- **B. Implementation and Reproducibility Details.**
Summary of experimental settings and reproducibility resources.
- **C. Continual Learning Metrics and CARA.**
Standard CL metrics (AvgACC, FAA, BWT, AvgF) and the proposed compute-adjusted metric CARA.
- **D. Model Size Analysis: Facebook/DINOv2.**
Comparison of model variants and justification for backbone selection.
- **E. UniPrompt-CL Training Procedure.**
We provide a detailed algorithmic description of the UniPrompt-CL training procedure in tabular form.

A GenAI Usage Disclosure

Although the authors carried out the overall code development and manuscript preparation, the conversion of the written manuscript into LaTeX, its proof-reading, and translation were performed using OpenAI’s ChatGPT, and code refactoring was assisted by Cursor.

B Implementation and Reproducibility Details

To ensure reproducibility and completeness, we summarize the datasets, experimental setup, and released resources for both the main DR study and supplementary external experiments.

Table 8: Distribution of datasets used for training

Dataset	Normal (0)	NPDR (1)	PDR (2)
APTOS [12]	1805	1562	295
DDR [21]	6266	5343	913
DRD [8]	5000	8608	708

Main datasets (Diabetic Retinopathy). Our primary experiments use three publicly available diabetic retinopathy (DR) datasets (APTOS, DDR, and

DRD). Since some benchmarks do not provide ground-truth labels for the official test sets, we follow prior work [18] to preprocess the data and construct consistent train/validation/test splits. As in [18], we remap the original five DR grades (normal, mild, moderate, severe, proliferative) into three clinically meaningful classes: normal, NPDR, and PDR, by merging mild/moderate/severe into NPDR while keeping normal and PDR unchanged. The final data distribution and dataset sources are summarized in Sup. Table 8. In our continual learning setting, the training stream is denoted as

$$D = \{D_1, D_2, \dots, D_n\}, \quad D_n = \{X_{n,b}, Y_{n,b}\},$$

where n is the stage index, $X_{n,b}$ is an input image, $Y_{n,b}$ is the corresponding label, and b indexes samples within a batch of size B .

Supplementary external datasets (Skin cancer). To assess generalization beyond DR, we conduct small-scale external experiments under the same domain-incremental protocol, using three skin-cancer datasets in the order ISIC \rightarrow HAM \rightarrow DERM7, yielding three stages. Following prior work on ISIC lesion grouping [4], we remap the original diagnostic categories into a clinically motivated binary setting: lesions requiring urgent clinical intervention are grouped as *malignant*, while others are grouped as benign. Dataset statistics and representative example images are provided in Sup. Tables 9 and Sup. Figure 4. All datasets are split 8:1:1 into train/validation/test sets. All other settings (model, training schedule, hyperparameters, and metrics) are identical to the DR study; only the datasets change, and we set the batch size to 16 due to the smaller dataset size.

Table 9: Distribution of datasets used for training

Dataset	Benign	Malignant
ISIC [29]	584	584
HAM [7]	1113	1113
DERM7 [13]	252	252

Implementation details. Our implementation uses Python 3.8 and PyTorch **2.4.1+cu118**. All experiments were conducted in the controlled environment summarized in Sup. Table 10 and Table 11. We used two NVIDIA V100 GPUs for training efficiency; however, the full GPU memory capacity was not required, since PCL methods update only additional learnable parameters while keeping most of the backbone frozen. In practice, training with a single V100 required approximately 8 GB VRAM, supporting reproducibility on modest hardware.

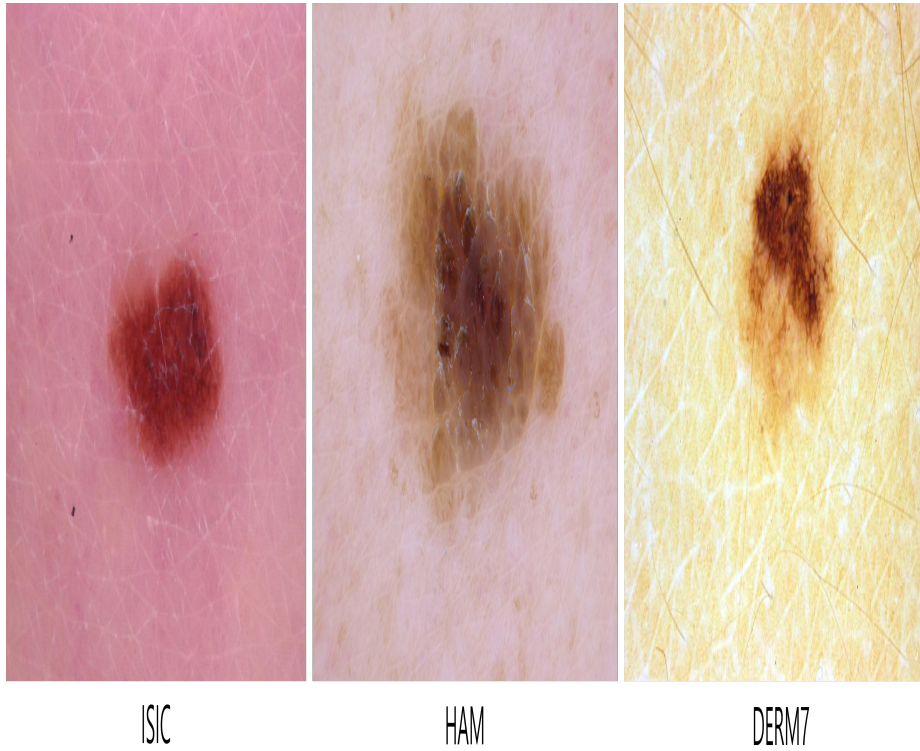


Fig. 4: Representative examples from the three skin cancer datasets used in our pilot study: ISIC [29], HAM [7], and DERM7 [13]. The samples illustrate the diversity in lesion appearance and acquisition conditions across datasets.

Table 10: Experiment Settings

Item	Value
GPU	$2 \times V100$
RAM	256GB
Learning Rate	0.001
Scheduler	Cosine Scheduler
Number of Prompts (L_p)	500
Prompt Dimension (D)	768
Optimizer	AdamW
Early Stop Patience	5
Epochs	100
Batch Size	64
Image Size	224×224

Table 11: Key hyperparameters for prompt-based continual learning baselines.

Method	Hyperparameter	Value
CODA-Prompt	Prompt pool size (<code>coda_pool_size</code>)	100
	Prompt length (<code>coda_prompt_length</code>)	4
	Ortho. regularization coeff. (<code>coda_ortho_mu</code>)	0.1
DualPrompt	Prompt length (<code>dual_prompt_length</code>)	4
	Prompt pool size (<code>dual_pool_size</code>)	100
	Top- k prompts (<code>dual_top_k</code>)	5
	G-prompt length (<code>dual_g_prompt_length</code>)	4
	G-prompt layers (<code>dual_g_prompt_layers</code>)	[0, 1]
	E-prompt layers (<code>dual_e_prompt_layers</code>)	[2, 3, 4]
DER++	Head type (<code>dual_head_type</code>)	token
	ALPHA (larger values emphasize preserving past knowledge)	0.5
	BETA (larger values emphasize relearning past tasks)	0.5
	BUFFER_SIZE (number of stored past samples)	30
Online EWC	RP_SIZE (dimension of the random projection matrix)	10000
	OPTIM_MOM (SGD momentum)	0.9
	OPTIM_WD (ℓ_2 regularization coefficient)	0.0005
MoE Adapters	PROMPT_TEMPLATE (CLIP text prompt template)	“a photo of { }.”
	CLIP_BACKBONE (CLIP model backbone)	ViTB/16
	VIRTUAL_BS_N (virtual batch size iterations)	1
OS (++) Prompt	Prompt Dim	768
	Pool size	150

C Continual Learning Metrics

$$\text{AvgACC} = \frac{1}{T} \sum_{i=1}^T \left(\frac{1}{i} \sum_{j=1}^i R_{i,j} \right). \quad (8)$$

Symbols: - T : total number of stages (or tasks) - $R_{i,j}$: accuracy on task j after training up to stage i

Explanation: This metric measures the average accuracy trajectory throughout the entire training process. After learning each task i , it computes the average accuracy over all tasks learned so far (from 1 to i), and then averages this value across all T tasks.

Meaning: AvgACC provides a comprehensive view of how stably the model maintains its performance over time. Unlike metrics that only evaluate the final result, it reflects performance consistency across the whole learning process.

$$\text{BWT} = \frac{1}{T-1} \sum_{j=1}^{T-1} (R_{T,j} - R_{j,j}). \quad (9)$$

Symbols: - T : total number of stages - $R_{j,j}$: accuracy on task j immediately after it was first learned - $R_{T,j}$: final accuracy on task j after completing all T stages

Explanation: BWT measures how the performance on past tasks changes after learning new tasks.

Meaning: - If $BWT \approx 0$, new tasks do not affect old tasks (no forgetting). - If $BWT < 0$, forgetting occurs. - If $BWT > 0$, new tasks improve the performance on old tasks, indicating *positive backward transfer*.

$$\text{AvgF} = \frac{1}{T-1} \sum_{j=1}^{T-1} \left(\max_{i \in \{j, \dots, T\}} R_{i,j} - R_{T,j} \right). \quad (10)$$

Symbols: - T : total number of stages (or tasks) - $R_{i,j}$: accuracy on task j after training up to stage i - $R_{T,j}$: final accuracy on task j after completing all T stages - $\max_{i \in \{j, \dots, T\}} R_{i,j}$: the best accuracy achieved on task j during the entire training process

Explanation: Average Forgetting (AvgF) measures how much performance is lost on previously learned tasks after completing all training stages. It compares the best performance achieved on each task during training with its final accuracy.

Meaning: - AvgF quantifies the extent of catastrophic forgetting across tasks. - A higher AvgF value indicates that the model has forgotten more knowledge from earlier tasks. - An AvgF close to 0 implies strong retention of previously learned knowledge.

$$\text{CARA}_p = \frac{\text{AvgACC} \times (1 - \text{AvgF})}{\text{GFLOPs}^p}, \quad p \in [0, 1]. \quad (11)$$

Symbols:

- AvgACC: average accuracy (0–1 scale)
- AvgF: average forgetting (0–1), lower is better
- $1 - \text{AvgF}$: *retention* (forgetting-adjusted performance)
- GFLOPs: inference compute cost (higher means more cost)
- p : strength of the compute penalty (typically $0.25 \sim 1.0$; default $p = \frac{1}{2}$)

Explanation: Cost-Adjusted Retained Accuracy (CARA) combines performance (AvgACC) and stability (retention = $1 - \text{AvgF}$) into a single “retained performance,” and normalizes it by a power of the compute cost GFLOPs ^{p} . It summarizes the trade-off among accuracy, forgetting, and efficiency.

Meaning:

- Larger values indicate **higher accuracy**, **lower forgetting**, and **reasonable compute** simultaneously.
- $p = \frac{1}{2}$ (CARA@ $\sqrt{\text{cost}}$): applies a mild penalty to compute, balancing performance/stability and efficiency (recommended default).
- $p \rightarrow 0$: almost ignores compute (compares retained performance only).
- $p \rightarrow 1$: penalizes compute linearly (prioritizes efficiency more).

D Model Size Analysis: facebook/dinov2

In this section, we explain the rationale for choosing the DINOv2-base model [24]. In general, models with a larger number of parameters can extract richer features and thus achieve better performance. However, as model size increases, the

Table 12: Parameter counts for facebook/dinov2 models

Model	Parameters
facebook/dinov2-small	22.1 M
facebook/dinov2-base	86.6 M
facebook/dinov2-large	304 M
facebook/dinov2-giant	1.14 B

parameter count grows more than twofold at each step, leading to significantly higher complexity. For this reason, we adopted the moderately sized DINOv2-base model. Remarkably, it still achieved substantially better performance compared to existing methods.

Sup. Table 12 summarizes the four variants of the facebook/dinov2 family in terms of model size and corresponding parameter counts, where M denotes millions of parameters and B denotes billions. These models were employed using the Hugging Face library.

E UniPrompt-CL Training Procedure

We present Sup.Algorithm 1, UniPrompt-CL Training Procedure (Fixed per-stage prompt expansion), to clarify the training process and the behavior of the model.

Algorithm 1 UniPrompt-CL Training Procedure (Fixed per-stage prompt expansion)

Require: Initial DINOv2 backbone \mathcal{M} ; initial prompt keys $K^{(0)}$; initial prompt values $P^{(0)}$; learning rate η ; epochs E ; batch size B ; dataset sequence $\{\mathcal{D}_n\}_{n=1}^N$; prompt expansion ratio ρ (e.g., 0.2); regularization weight λ_{reg} ; cosine similarity function $\gamma(\cdot)$; number of dataset N ; sequence of ViT layer l ;

Ensure: Trained model \mathcal{M} and unified prompt pool (K, P) As the sequence of stages progresses, the model \mathcal{M} is continually updated, i.e., incrementally trained at each stage.

```

1:  $K \leftarrow K^{(0)}, P \leftarrow P^{(0)}$ 
2:  $N_0 \leftarrow |K|, N_{\text{add}} \leftarrow \lfloor N_0 \cdot \rho \rfloor, N_{\text{tot}} \leftarrow N_0$ 
3: for  $n = 1$  to  $N$  do
4:    $\mathcal{D} \leftarrow \mathcal{D}_n$ 
5:   if  $n > 1$  then
6:     freeze  $K[1 : N_{\text{tot}}]$  and  $P[1 : N_{\text{tot}}]$ 
7:      $\Delta K \leftarrow \text{RandomInit}(N_{\text{add}}, d); \Delta P \leftarrow \text{RandomInit}(N_{\text{add}}, d)$ 
8:      $K \leftarrow K \cup \Delta K; P \leftarrow P \cup \Delta P$ 
9:      $N_{\text{tot}} \leftarrow N_{\text{tot}} + N_{\text{add}}$ 
10:  end if
11:   $\text{Opt} \leftarrow \text{AdamW}(\{\theta_{\mathcal{M}}, \theta_{\Delta K}, \theta_{\Delta P}\}, \eta)$ 
12:   $\text{Sched} \leftarrow \text{CosineScheduler}(\text{Opt}, T_{\text{max}} = E)$ 
13:  for  $e = 1$  to  $E$  do
14:    for each mini-batch  $(X, Y) \sim \mathcal{D}$  of size  $B$  do
15:       $z_{\text{list}} \leftarrow []$ 
16:       $x \leftarrow X$ 
17:       $p^* \leftarrow \text{NormalizeBatchPrompt}(P)$ 
18:      for  $\ell = 1$  to  $l_{\text{use}}$  do
19:         $x \leftarrow \mathcal{M}_{\ell}(x)$ 
20:         $q_{\ell} \leftarrow \text{CLS}(x)$ 
21:         $\phi_{\ell} \leftarrow \gamma(q_{\ell} K) P$ 
22:         $x_{\text{next}} \leftarrow f_{\ell}(x, \phi_{\ell})$ 
23:         $x \leftarrow x_{\text{next}}$ 
24:         $z_{\ell} \leftarrow \text{Softmax}\left(\frac{K(p^*)^{\top}}{\|K\| \|p^*\|}\right)$ 
25:        append  $z_{\ell}$  to  $z_{\text{list}}$ 
26:      end for
27:      for  $\ell = l_{\text{use}} + 1$  to  $l_{\text{total}}$  do
28:         $x \leftarrow \mathcal{M}_{\ell}(x)$ 
29:      end for
30:       $\hat{Y} \leftarrow \text{Classifier}(x)$ 
31:       $\mathcal{L}_s \leftarrow \mathcal{U}(z_{\text{list}})$  (defined in Eq. (6))
32:       $\mathcal{L}_{\text{CE}} \leftarrow \text{CrossEntropy}(\hat{Y}, Y)$ 
33:       $\mathcal{L}_{\text{total}} \leftarrow \mathcal{L}_{\text{CE}} + \lambda_{\text{reg}} \mathcal{L}_s$ 
34:      Backpropagate  $\nabla \mathcal{L}_{\text{total}}; \text{Opt.step}()$ 
35:    end for
36:     $\text{Sched.step}()$ 
37:  end for
38:   $\text{Eval}(n) \leftarrow \text{Evaluate\_Tests}(\mathcal{M}, \{\mathcal{D}_n\}_{n=1}^N)$ 
39: end for
40: return  $\mathcal{M}, (K, P)$ 

```
